# Wet Chemistry Self-Seeded Surface-Deposition Process toward Amorphous Carbon Nanotubes and Their Electrochemical Application

Jian-Min Shen, Lin Xu, Yu-Ge Liu, Chun-Liang Lu, Wen-Hua Hou,* and Jun-Jie Zhu*

*Key Laboratory of Mesoscopic Chemistry (MOE), Key Laboratory of Analytical Chemistry for Life Science (MOE), School of Chemistry and Chemical Engineering, Nanjing University, China*

*Received October 15, 2007. Revised Manuscript Received March 4, 2008*

In this paper, bunches of amorphous carbon nanotubes (α-CNTs) have been successfully synthesized on a large scale from a solution-based reaction between ferrocene and carbon tetrachloride at 180 °C for 12 h. The α-CNT is 3−5 $\mu$m in length and ∼300/200 nm in diameter (outer/inner) and has a Brunauer–Emmett–Teller (BET) specific surface area of 431 $m^2\ g^{-1}$ with a narrow pore distribution centered at 4.03 nm. The as-prepared α-CNTs showed a reversible capacity of ∼302 mA h $g^{-1}$ and little hysteresis in the charge/discharge experiments of secondary lithium ion batteries, which suggested that the α-CNTs might become a new candidate as an electrode material in secondary lithium-ion batteries. Herein, a possible self-seeded surface-deposition growth mechanism of these α-CNTs has been proposed. This mechanism is of importance to understand the nucleation process in the solution phase and growth of other nanotubes through a similar seeded deposition process.

## Introduction

In recent years, porous carbon materials have attracted considerable research interest due to their applications in many areas including pollutant purification, gas separation and storage, catalyst–support, and electrochemical devices.[1,2] Great progress has been achieved in the preparation of two major types of porous carbon materials, mesoporous carbon molecular sieves and amorphous carbon nanotubes (α-CNT).

Carbon nanotubes have been one of the most intensively studied materials because of their unique properties and potential impact in broad areas since their discovery in 1991.[3] Numerous efforts have been devoted to the fabrication of carbon nanotubes and exploration of the theory that dominates the formation process. Thus far, many synthetic strategies, such as arc discharge,[4] laser ablation,[5] chemical vapor deposition (CVD),[6] and solvothermal method,[7,8] have been developed to generate carbon nanotubes with "well-crystallized" tube walls through the classical vapor–liquid–solid (VLS) mechanism.

As an important porous carbon nanostructure, α-CNT has been realized through various novel approaches. Zhao et al. prepared α-CNT through arc discharge in hydrogen atmosphere and discussed the influence of temperature and catalyst on the final products.[9] Peng et al. produced α-CNTs by pyrolysis of organic species in anodic aluminum oxide (AAO) template.[10] Ci et al. obtained α-CNTs by CVD method and discussed their crystallization behavior.[11] Nishino, Otero-Díaz, and co-workers reported formation of various amorphous carbon nanostructures, including carbon nanotubes, hollow and solid nanospheres, through the fluorination of ferrous chloride[12,13] or direct chlorination of metallocene[14–17] at high temperatures in the vapor phase. They found that the crystallized Fe species, such as $FeCl_3$, $FeCl_2$, and $FeF_2$, served as carbon transport media or hard

* To whom correspondence should be addressed. W.-H.H.: phone, +86-25-83686001; fax, +86-25-83317761; e-mail, whou@nju.edu.cn. J.-J.Z.: phone/fax, +86-25-83594976; e-mail, jjzhu@nju.edu.cn.

(1) Ryoo, R.; Joo, S. H.; Kruk, M.; Jaroniec, M. *Adv. Mater.* **2001**, *13*, 677.
(2) Lu, K.; Chung, D. D. L. *Carbon* **1997**, *35*, 427.
(3) Iijima, S. *Nature* **1991**, *354*, 56.
(4) Jonrnet, C.; Maser, W. K.; Bernier, P.; Loiseau, A.; Lamy de la Chapelle, M.; Lefrant, S.; Deniard, P.; Lee, R.; Fischer, J. E. *Nature* **1997**, *388*, 756.
(5) Thess, A.; Lee, R.; Nikolaev, P.; Dai, H. J.; Petit, P.; Robert, J.; Xu, C. H.; Lee, Y. H.; Kim, S. G.; Rinzler, A. G.; Colbert, D. T.; Scuseria, G. E.; Tomanek, D.; Fischer, J. E.; Smalley, R. E. *Science* **1996**, *273*, 483.
(6) Cheng, H. M.; Li, F.; Sun, X.; Brown, S. D. M.; Pimenta, M. A.; Marucci, A.; Dresselhaus, G.; Dresselhaus, M. S. *Chem. Phys. Lett.* **1998**, *289*, 602.
(7) Jiang, Y.; We, Y.; Zhang, S. Y.; Xu, C. Y.; Yu, W. C.; Xie, Y.; Qian, Y. T. *J. Am. Chem. Soc.* **2000**, *122*, 12383.
(8) Liu, J. W.; Shao, M. W.; Chen, X. Y.; Yu, W. C.; Liu, X. M.; Qian, Y. T. *J. Am. Chem. Soc.* **2003**, *125*, 8088.
(9) Zhao, T. K.; Liu, Y. N.; Zhu, J. W. *Carbon* **2005**, *43*, 2907.
(10) Hu, Z. D.; Hu, Y. F.; Chen, Q.; Duan, X. F.; Peng, L.-M. *J. Phys. Chem. B* **2006**, *110*, 8263.
(11) Ci, L. J.; Wei, B. Q.; Xu, C. L.; Liang, J.; Wu, D. H.; Xie, S. S.; Zhou, W. Y.; Li, Y. B.; Liu, Z. Q.; Tang, D. S. *J. Cryst. Growth* **2001**, *233*, 823.
(12) Nishino, H.; Yamaguchi, C.; Nakaoka, H.; Nishida, R. *Carbon* **2003**, *41*, 2165.
(13) Nishino, H.; Nishida, R.; Matsui, T.; Kawase, N.; Mochida, I. *Carbon* **2003**, *41*, 2819.
(14) Urones-Garrote, E.; Ávila-Brande, D.; Ayape-Katcho, N.; Gómez-Herrero, A.; Landa-Cánovas, A. R.; Otero-Díaz, L. C. *Carbon* **2005**, *43*, 978.
(15) Urones-Garrote, E.; Ávila-Brande, D.; Katcho, N. A.; Gómez-Herrero, A.; Landa-Cánovas, A. R.; Lomba, E.; Otero-Díaz, L. C. *Carbon* **2007**, *45*, 1699.
(16) Ávila-Brande, D.; Urones-Garrote, E.; Katcho, N. A.; Lomba, E.; Gómez-Herrero, A.; Landa-Cánovas, Á. R.; Otero-Díaz, L. C. *Micron* **2007**, *38*, 335.
(17) Katcho, N. A.; Urones-Garrote, E.; Ávila-Brande, D.; Gómez-Herrero, A.; Urbonaite, S.; Csillag, S.; Lomba, E.; Agulló-Rueda, F.; Landa-Cánovas, Á. R.; Otero-Díaz, L. C. *Chem. Mater.* **2007**, *19*, 2304.

10.1021/cm702966x CCC: $40.75 
Published on Web 04/10/2008

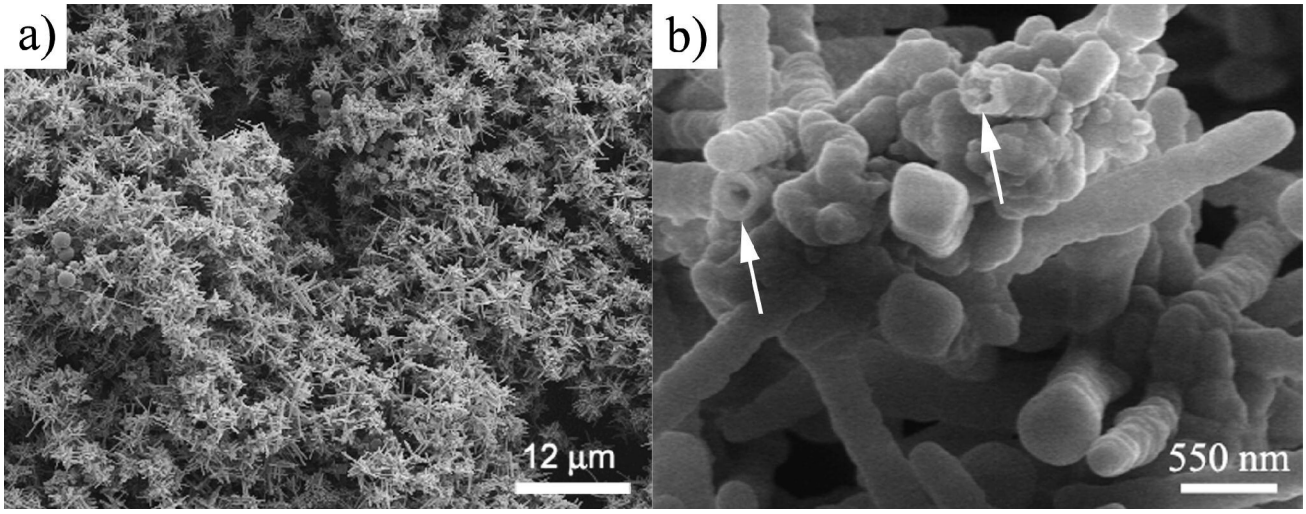


**Figure 1.** (a) FESEM image of the final product. (b) Close observation of a bunch of 1-dimensional nanostructures; broken tips are marked with arrows.

template for the formation of various carbon nanostructures. Recently, Qian and Xie's groups developed a number of mild solvothermal systems to synthesize α-CNTs with various structures and explored their formation mechanisms.[18,19]

Analogous to the VLS growth process of crystallized nanowires and nanotubes in the gas phase at high temperatures, a novel solution−liquid−solid (SLS) theory was established and successfully applied to elucidate formation of nanotubes including tellurium, selenium, and titania in the solution phase under much milder conditions.[20–22] However, to the best of our knowledge, formation of carbon nanotubes through a similar "colloid-seeded deposition" process in solution has seldom been reported. In the present work, we demonstrate an efficient method to produce α-CNTs through a self-seeded solution-based approach and explore their electrochemical applications.

## Experimental Section

In a typical experiment, 0.4 g of ferrocene ($Fe(C_5H_5)_2$) (AR) was first dissolved into 50 mL of carbon tetrachloide ($CCl_4$) (AR) to form a transparent solution. Then the solution was transferred into a Teflon-lined stainless steel container to about 85% of its total volume. The container was sealed, kept at 180 °C for 12 h, and then cooled down to room temperature naturally. A black product was filtered out and washed with distilled water and absolute ethanol several times before it was dried in a vacuum at 80 °C for 8 h.

Field emission scanning electron microscope (FESEM) images were taken on a JEOL JSM-6300F SEM. Transmission electron microscopy, high-resolution TEM (HRTEM) images, selected-area electron diffraction (SAED) patterns, energy-dispersive X-ray spectra (EDS), and electron energy-loss spectra (EELS) were obtained on a JEM-2010F high-resolution transmission electron microscope equipped with EDS and EELS detectors working at an acceleration voltage of 200 kV. The X-ray powder diffraction (XRD) analysis was performed with a Philips X" Pert PRO SUPER XRD diffractometer ($\lambda = 0.1541874$ nm). Room-temperature Raman spectra were recorded on a Spex 1403 Raman spectrometer ($\lambda = 514.5$ nm). Specific surface areas were measured on Micromeritics ASAP 2020 nitrogen adsorption equipment at liquid nitrogen temperature. The electrochemical performance of the product as an electrode was measured using a Teflon cell with a lithium metal anode. The cathode was prepared by mixing α-CNTs and poly(vinylidene fluoride) at a weight ratio of 9:1. The electrolyte was 1 M $LiPF_6$ in a 1:1 mixture of ethylene carbonate and diethyl carbonate. The separator was Celgard 2320. The cells were cycled galvanostatically from 2.5 to 0.1 V at current densities of 50, 100, and 200 mA $g^{-1}$, respectively, on a Land battery system (CT2001A). All the electrochemical experiments were carried out at ambient temperature in a glovebox purged with pure argon ($O_2$ and $H_2O$ levels < 5 ppm).

## Results and Discussion

Field emission scanning electron microscopy (FESEM) characterization of the as-prepared sample is shown in Figure 1. Most of the final product is composed of bunches of rod-like nanostructures with a length of 3–5 $\mu$m and a diameter of 300 nm. Only a few particles exist in the product, and the percentage of the rod-like nanostructure is over 85%. Figure 1b is a detailed observation of one bunch of the rod-like nanostructures with round and closed tips. However, as shown in the image, a few rod-like nanostructures with broken tips have hollow interiors, exhibiting a tubular nanostructure.

To provide further insight into the microstructure and morphology of the product, transmission electron microscopy (TEM) analysis was applied to examine the sample. A TEM image in Figure 2a shows several clusters of nanotubes in which the tubular nanostructures with closed tips can be clearly distinguished from the obvious contrast difference

(18) Luo, T.; Chen, L. Y.; Bao, K. Y.; Yu, W. C.; Qian, Y. T. *Carbon* **2006**, *44*, 2844.
(19) Xiong, Y. J.; Xie, Y.; Li, X. X.; Li, Z. Q. *Carbon* **2004**, *42*, 1447.
(20) Mayers, B.; Xia, Y. *Adv. Mater.* **2002**, *14*, 279.
(21) Xi, G. C.; Xiong, K.; Zhao, Q. B.; Zhang, R.; Zhang, H. B.; Qian, Y. T. *Cryst. Growth Des.* **2006**, *6*, 577.
(22) Lin, Y.; Gao, W.; Zhang, D. Y.; Guo, X. F.; Ding, W. P.; Chen, Y. *J. Am. Chem. Soc.* **2006**, *128*, 11042.

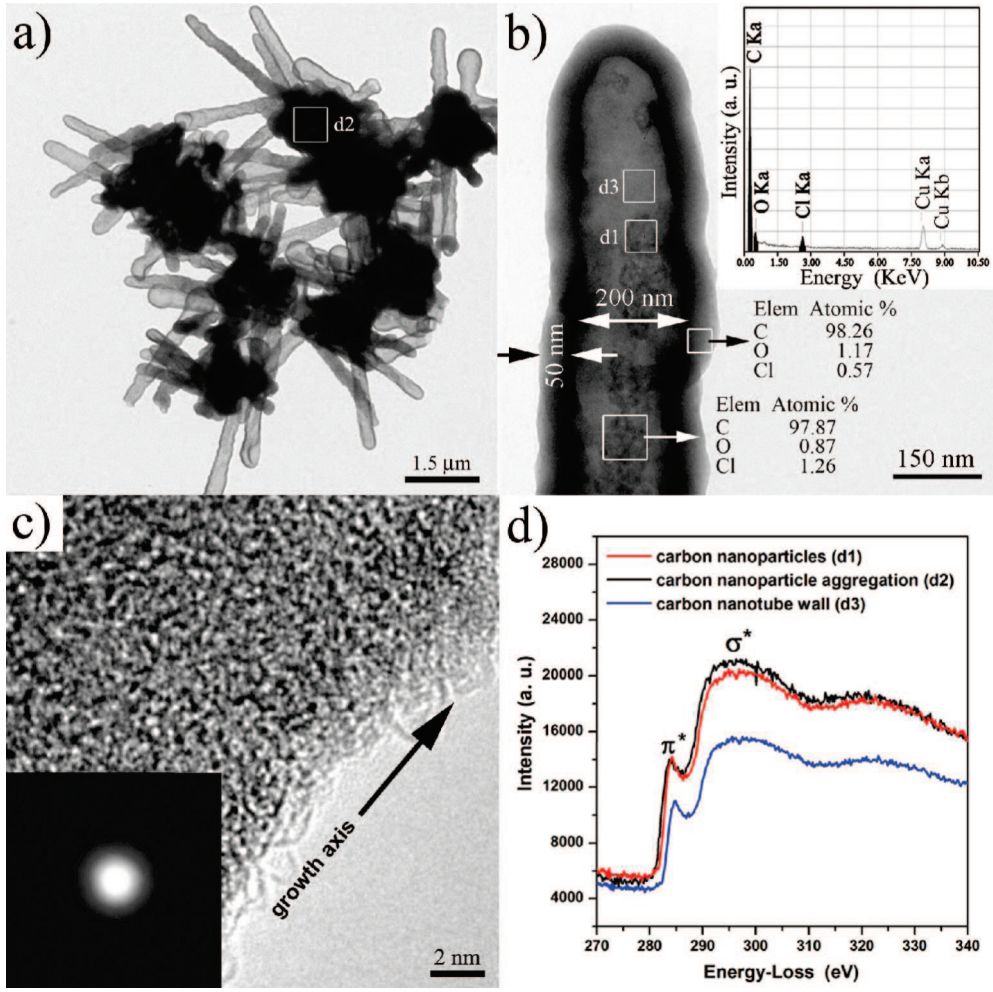


**Figure 2.** (a) Low-magnified TEM image of the final product. (b) Elemental analysis results of the wall and its inside nanoparticles of one nanotube; (inset) EDS spectrum. (c) HRTEM image of the wall structure of a carbon nanotube; (inset) corresponding ED pattern. (d) EELS analysis results of carbon nanotube wall, inside carbon nanoparticle, and carbon nanoparticle aggregate at the root of the carbon nanotube.

between the dark tube wall and gray inside. However, it is worth noting that a cluster of nanotubes is generated from some tips of a common "root". Figure 2b typically depicts a TEM image of a nanotube with an average inner diameter of ~200 nm, a wall thickness of ~50 nm, and some inside nanoparticles with a diameter of ~10 nm. The X-ray energy-dispersive spectrum (EDS), inset of Figure 2b, shows that both the as-prepared nanotube and the inside nanoparticles are mainly composed of carbon with a little oxygen and chlorine (copper signals are from the copper grid support). A similar spectrum and elemental composition can also be obtained from the microparticle at the root of a cluster of carbon nanotubes (Figure S1, Supporting Information). Although further elemental analysis and TEM examination cannot detect the signals of Fe or its species from the untreated raw α-CNTs or their root part (Figure S2, Supporting Information), we do not exclude the possible involvement of Fe species in the growth process of the carbon nanotubes. The existence of carbon nanoparticles inside the nanotubes is not in accordance with previous literature results[12–17] and implies a different growth mechanism of these α-CNTs. Moreover, a superior chlorine content of the inside carbon nanoparticles to that of the tube wall might be attributed to their different formation processes and the relatively enclosed tubular nanostructure, which protects the adsorbed chlorine from dissipation in the TEM examination. Figure 2c reveals that the nanotube wall is almost completely composed of amorphous or disordered structures through high-resolution TEM (HRTEM) inspections. The inset of Figure 2c, a selected area electron diffraction (SAED) pattern obtained by perpendicularly focusing the incident electron beam on the carbon nanotube, shows only one weak and dispersive spot, which is also typical of amorphous structures.

The electron energy-loss spectrum (EELS) analysis was carried out to provide further insight into the bonding information between carbon atoms in α-CNTs. Representative EELS results in Figure 2d, showing the $\pi^*$ and $\sigma^*$ signals, are the energy-loss near-edge structure (ELNES) spectra corresponding to the carbon-K adsorption edge obtained at different positions of the final product. The peak at around 285 eV can be attributed to the transition from carbon 1s to the antibonding $\pi^*$ states, typical of $sp^2$-bonded carbon, while the other broad peak at 290–310 eV is associated with the transition from carbon 1s to $\sigma^*$ states of $sp^3$-bonded carbon.[10,23] Although the fine structure of the

(23) Suenaga, K.; Sandrél, E.; Colliex, C.; Pickard, C. J.; Kataura, H.; Iijima, S. *Phys. Rev. B* **2001**, *63*, 165408.

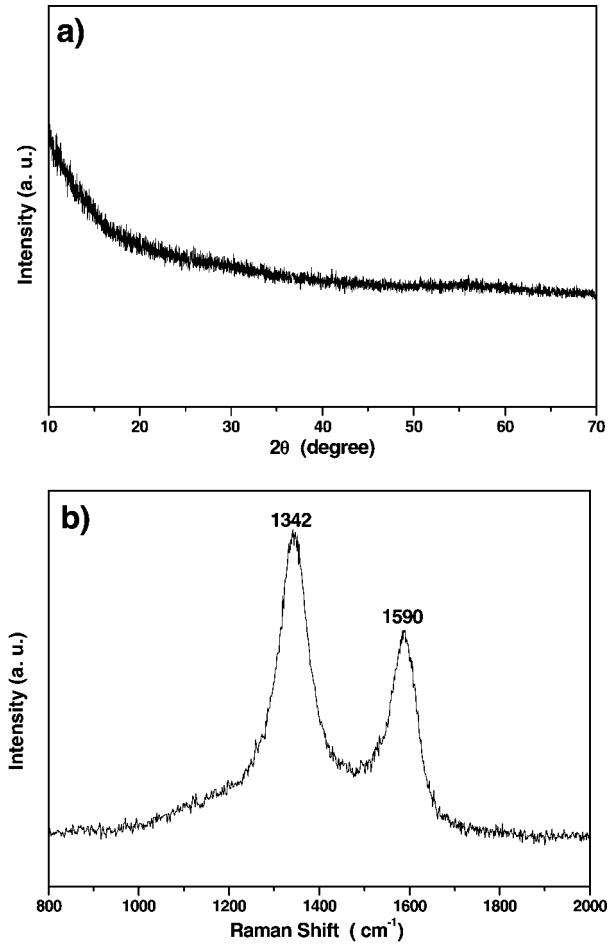


**Figure 3.** (a) XRD pattern and (b) room-temperature Raman spectrum of the final product.

adsorption edges indicates that the root of the α-CNTs (area d2), the tube wall (area d3), and its inside nanoparticles (area d1) are typical of amorphous carbon, the intensities of $\pi^*$ and $\sigma^*$ peaks in carbon ELNES spectra are often dependent on the structural anisotropy of different regions where they were collected.[24] Thus, the different $\pi^*/\sigma^*$ ratios of spectra d1 and d3, obtained on two adjacent areas with similar anisotropy from the tube wall and the inside nanoparticles in Figure 2b, can only be attributed to their different microstructures.

Powder X-ray diffraction (XRD) and Raman spectroscopy were used to study the phase purity and microstructure of the final product, respectively. As shown in Figure 3a, the XRD pattern of the final product shows no prominent peak at all, indicating a completely amorphous phase, which is consistent with the results from HRTEM and SAED analysis. Signals induced by impurities are below the instrument detection limit (<5%). The Raman spectrum in Figure 3b exhibits two strong peaks at 1342 (D band) and 1590 $cm^{-1}$ (G band), respectively, which are the characteristics of carbon nanotube vibration modes. The G-band peak at 1590 $cm^{-1}$ corresponds to the Raman $E_{2g}$ mode of graphite and is closely related to the vibration of $sp^2$-bonded carbon atoms within

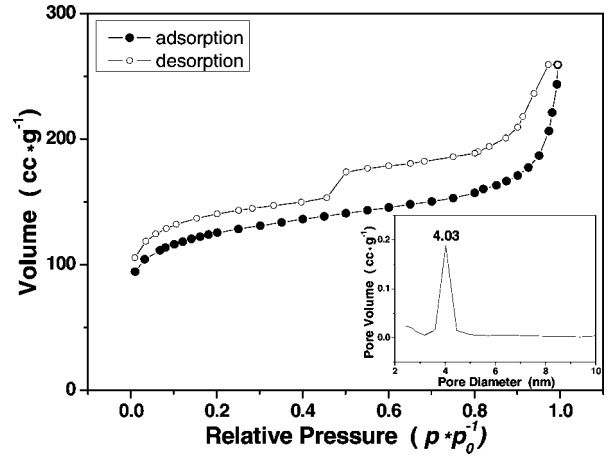


**Figure 4.** Nitrogen adsorption/desorption isotherms of the final product; (inset) BJH pore-size distribution curve.

the hexagonal graphitic plane, while the broad D-band peak at 1342 $cm^{-1}$ ($A_{1g}$ mode) can be attributed to vibration of carbon atoms with dangling bonds at the edges or defects of graphitic lattice.[25] The superior intensity of the D-band peak to that of the G-band peak in Raman spectroscopy indicates that the final product is poorly graphitized, in accordance with the HRTEM observation. Similar results have also been reported in previous inspections of various amorphous carbon nanostructures.[19]

Figure 4 and its inset are the representative nitrogen adsorption/desorption isotherms and corresponding Barrett–Joyner–Halenda (BJH) pore-size distribution curve of the as-prepared carbon product, respectively. The nitrogen sorption isotherm can be classified as type IV with an open H4-type hysteresis loop,[26] which often results from the mesoporous structures such as aggregation of particles.[17] The pore-size distribution of α-CNTs, calculated from nitrogen desorption using the BJH model, shows a narrow distribution centered at 4.03 nm. According to the results of nitrogen adsorption, the total BET surface area of the sample is calculated to be 431 $m^2\ g^{-1}$, which is much higher than that of graphitized multiwalled carbon nanotubes with similar microstructure and carbon nanospheres (10–20 $m^2\ g^{-1}$).[27,28] The result can be largely attributed to the abundant microporosities (Figure S3, Supporting Information) and mesoporosities inside the carbon nanoparticle aggregates. The 4.03 nm pore size is close to the calculated diameter of the octahedron interstices (4.14 nm) among the closely packed carbon nanoparticles with a unique diameter of ∼10 nm inside their micrometer-sized aggregations at the root part of a bunch of carbon nanotubes.

The obtained α-CNTs possess high BET values, tubular microstructures, and highly disordered tube walls, which are expected to increase the active sites for lithium intercalation

(24) Egerton, R. F. *Electron Energy-loss Spectroscopy in the Electron Microscope*; Plenum Press: New York, 1996.
(25) Dresselhaus, M. S.; Dresselhaus, G.; Pimenta, M. A.; Eklund, P. C. *Analytical Applications of Raman Spectroscopy*; Blackwell Science: Oxford, 1999.
(26) Sing, K. S. W.; Everett, D. H.; Haul, R. A. W.; Moscou, L.; Pierotti, R. A.; Rouquerol, J.; Siemieniewska, T. *Pure Appl. Chem.* **1985**, *57*, 603.
(27) Ajayan, P. M. *Chem. Rev.* **1999**, *99*, 1787.
(28) Peigney, A.; Laurent, Ch.; Flahaut, E.; Bacsa, R. R.; Rousset, A. *Carbon* **2001**, *39*, 507.

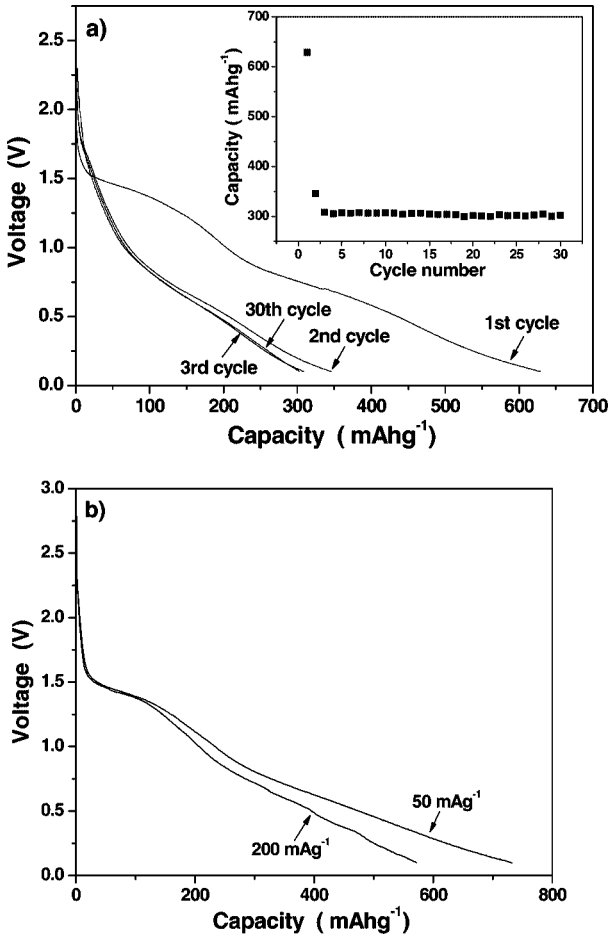


**Figure 5.** (a) Voltage versus discharge capacity curves for the α-CNT/Li cell between 2.5 and 0.1 V at the 1st, 2nd, 3rd, and 30th cycles, respectively; (inset) corresponding cyclic performances for the α-CNT/Li cell. (b) First discharge capacity curves of the α-CNT electrodes at current densities of 50 and 200 mA $g^{-1}$.

and thus improve the electrode performance in a $Li^+$ secondary battery.[29,30] The voltage profile of a α-CNT/Li cell in the discharge curves (Figure 5a) shows the electrochemical discharge behavior with the voltage of 0.1–2.5 V. When $Li^+$ inserts into the α-CNTs in the first discharge, two sloping potential ranges (1.2–0.8 and 0.6–0.1 V versus $Li^+$/Li) can be discerned. It is generally accepted that the first slope could be attributed to decomposition of the electrolyte and formation of the solid electrolyte interphase (SEI) layer at the surface of the α-CNTs electrode,[31,32] while the second slope is related with insertion of $Li^+$ into α-CNTs. As shown in Figure 5a, the capacity of α-CNT is 629.1 mA h $g^{-1}$ for the first discharge and 346.2 mA h $g^{-1}$ for the second discharge, which indicates a capacity retention of 55.0%. The irreversible capacity can be largely concerned with decomposition of electrolyte and formation of the SEI layer, which are specifically enhanced with the increasing specific surface

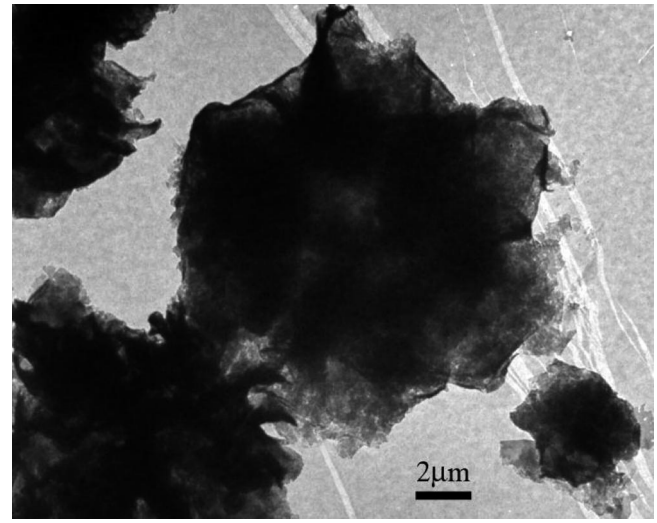


**Figure 6.** TEM image of the typical product by refluxing the mixture of ferrocene and carbon tetrachloride at 180 °C for 12 h.

area and structural disorder in carbonaceous materials.[33] The inset reveals that the capacity curve reaches a plateau after three charge/discharge cycles and stays relatively invariable up to the 30th cycle at 302.3 mA h $g^{-1}$ at a current density of 100 mA $g^{-1}$. The capacity is superior to that of the graphitized multiwalled carbon nanotubes (200–250 mA h $g^{-1}$) in previous reports.[34–36] The steady performance of the electrode suggests that insertion/extraction of $Li^+$ produces high reversibility and little hysteresis.

We further studied the $Li^+$ ion insertion performance of the α-CNT electrode by discharging the assembled cells at various current densities from 50 to 200 mA $g^{-1}$. Figure 5b shows the voltage versus the first discharge capacity of the electrode between 2.5 and 0.01 V at 50 and 200 mA $g^{-1}$, respectively. Compared with the aforementioned data obtained at a current density of 100 mA $g^{-1}$, the phenomenon that the first discharge capacity of a α-CNT/Li cell increases to 731.3 mA h $g^{-1}$ at a lower current density of 50 mA $g^{-1}$ and decreases to 571.6 mA h $g^{-1}$ at a higher current density of 200 mA $g^{-1}$ can be discerned in the profiles. The results indicate that the performance of the α-CNT electrode does not change dramatically at different current densities, which suggests potential application of the α-CNT electrode in areas that require fine stability for various current densities.

In the reaction process, the sealed solvothermal environment was essential to formation of carbon nanotubes. No carbon nanotubes could be obtained in a series of supplementary experiments carried out by refluxing carbon tetrachloride containing different amounts of ferrocene (0.08–0.4 g) at various temperatures (110–180 °C). A TEM image in Figure 6depicts that the product is composed of carbon microparticles, which are aggregates of many tiny carbon

(29) Besenhard, J. O. *Progress in Intercalation Research*; Kluwer: Dordrecht, The Netherlands, 1994.
(30) Winter, M.; Besenhard, O. J.; Spahr, M. E.; Novak, P. *Adv. Mater.* **1998**, *10*, 725.
(31) Wang, Q.; Liu, L. J.; Chen, L. Q.; Huang, X. J. *J. Electrochem. Soc.* **2004**, *151*, A1333.
(32) Maurin, G.; Bousquet, C.; Henn, F.; Bernier, P.; Almairac, R.; Simon, B. *Chem. Phys. Lett.* **1999**, *312*, 14.
(33) Matusumura, Y.; Wang, S.; Mondori, J. *J. Electrochem. Soc.* **1995**, *142*, 2914.
(34) Frackowiak, E.; Gautier, S.; Gaucher, H.; Bonnamy, S.; Beguin, F. *Carbon* **1999**, *37*, 61.
(35) Gao, B.; Kleinhammes, A.; Tang, X. P.; Bower, C.; Fleming, L.; Wu, Y.; Zhou, O. *Chem. Phys. Lett.* **1999**, *307*, 153.
(36) Wu, G. T.; Wang, C. S.; Zhang, X. B.; Yang, H. S.; Qi, Z. F.; He, P. M.; Li, W. Z. *J. Electrochem. Soc.* **1999**, *146*, 1696.

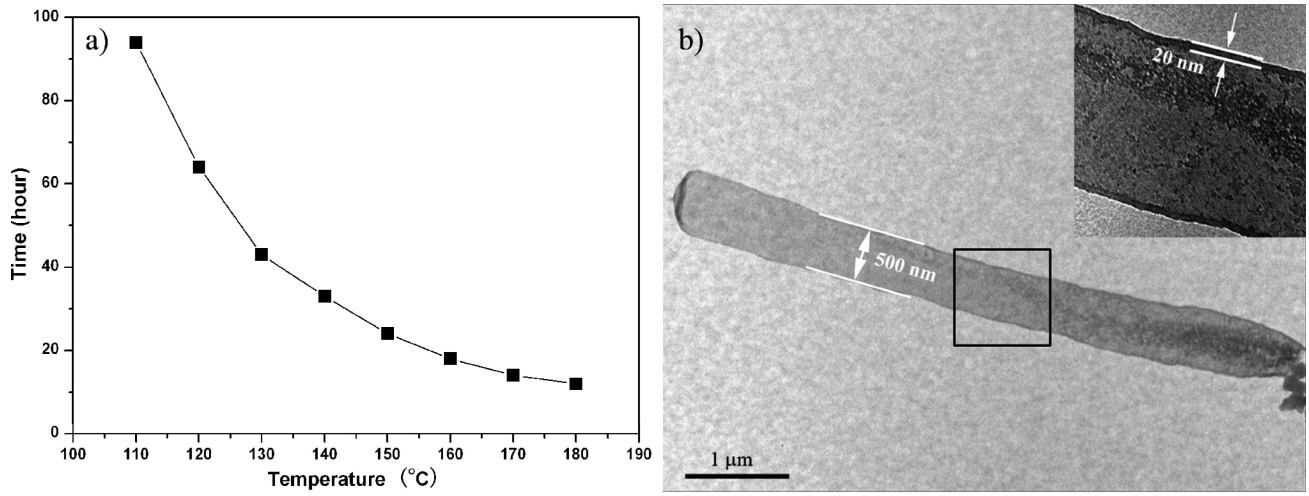


**Figure 7.** (a) Relationship between the reaction temperature and reaction time. (b) Typical TEM image of a carbon nanotube produced at 110 °C; (inset) magnified image of the tube wall.

nanoparticles. Previous reports on the preparation of 1-dimensional carbon nanomaterials from ferrocene through a wet chemistry approach indicated that the solvothermal technique could provide favorable conditions, such as temperature and pressure, for cyclopentadienyl anions to further break down to release carbon.[18,19,37] Although ferrocene can react with carbon tetrachloride to produce carbon microparticles by refluxing their mixture at an appropriate temperature, failure in introducing extra pressure cannot make the degradation of cyclopentadienyl groups take place and provide carbon feed stock for growth of carbon nanotubes. Thus, no carbon nanotubes can be obtained through refluxing.

The experimental parameters, such as the quantity of ferrocene and reaction temperature, also have a great influence on the structure and morphology of the product. In a series of experiments, we found that the length, outer diameter, and wall thickness of the carbon nanotubes would significantly decline as the amount of ferrocene reduces from 0.4 to 0.08 g. Instead of carbon nanotubes, only carbon nanoparticles with diameters of about 80 nm can be obtained once the quantity of ferrocene is below 0.08 g. The reaction between ferrocene and carbon tetrachloride not only generates sufficient carbon microparticles as deposition sites but also, more importantly, provides adequate carbon feed stock for the following growth of carbon nanotubes as well. The absence of tubular nanostructures can be attributed to insufficient carbon feed stock produced from less ferrocene and thus failure of carbon feed stock to cover the surfaces of the carbon microparticles and further develop into α-CNTs. The temperature is also a crucial factor in the growth process of α-CNTs, and the reaction is triggered only above 110 °C. Figure 7a shows an inverse relationship between the reaction temperature and time required to finish the reaction, which reveals that the higher the temperature is elevated, the faster the reaction is finished. However, the influence of reaction temperature is not only on the reaction rate but also on the structure of carbon nanotubes, such as the diameter and wall thickness. Shown in Figure 7b is a typical TEM image of a carbon nanotube produced at 110 °C. Compared with the product obtained at 180 °C, the carbon nanotube prepared at a lower temperature has an increased diameter from ~300 to 500 nm, while its wall thickness decreases from ~50 to 20 nm. The changes in carbon nanotube structure may result from the slow decomposition rate of cyclopentadienyl groups at low temperature, which leads to insufficient carbon feed stock in the system. Thus, carbon nanoparticle aggregates can grow their sizes to a larger extent before they are covered with a layer of carbon. When less carbon feed stock continues to deposit at a larger surface to support the growth of carbon nanotube, as shown in the inset of Figure 7b, the wall thickness has to be decreased. This phenomenon suggests that the microstructures of the α-CNTs are determined by the production of carbon feed stock and size of the deposition sites that are generated in situ in the solvothermal environment.

For an overview of the formation process and growth mechanism of nanotubes, a time-dependent morphology evolution examination was conducted on a series of intermediate products from 2 to 8 h at 180 °C. The corresponding TEM images are shown in Figure 8. When the system reacts for 2–3 h, the product is mainly composed of microparticles with irregular surfaces (Figure 8a). Six hours later, a bunch of short nanotubes (0.4–1.0 $\mu$m in length) with diameters of 300/200 nm (outer/inner) and close ends develop from the tips at the surface of the carbon microparticle (Figure 8b). As shown in the image, the inside of the nanotubes are densely filled with small carbon nanoparticles. Keeping their diameter and wall thickness almost unchanged, the elongated bunches of nanotubes (2 $\mu$m in length) with microparticles as their roots (Figure 8c) appear at a prolonged time of reaction (~8 h). The whole process is the directional growth of carbon nanotubes and similar to the seeded deposition in SLS growth of 1-D materials.[20–22]

The formation process of the α-CNTs under mild solvothermal conditions is intriguing, and a possible self-seeded surface-deposition growth mechanism is proposed based on

(37) Wu, C. Z.; Zhu, X.; Ye, L. L.; OuYang, C. Z.; Hu, S. Q.; Lei, L. Y.; Xie, Y. *Inorg. Chem.* **2006**, *45*, 8543.

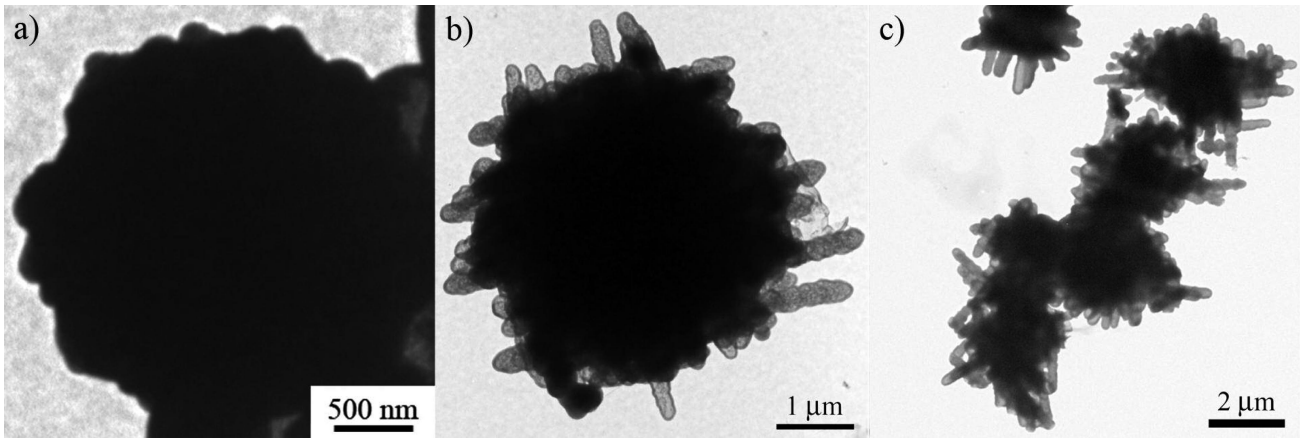


**Figure 8.** TEM images of the intermediate products from the reaction at (a) 2–3, (b) 6, and (c) 8 h.

**Scheme 1. Formation Process of a Bunch of Amorphous Carbon Nanotubes**[a]

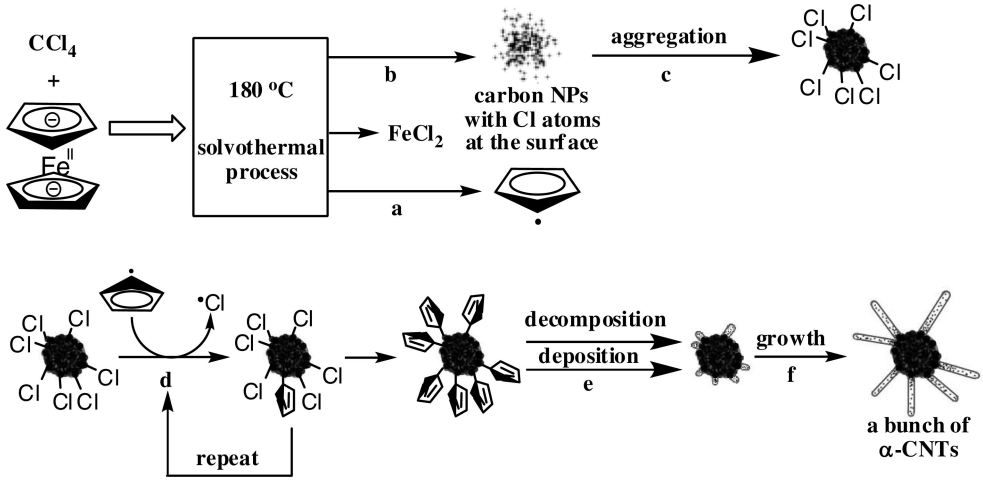


[a] The reaction between ferrocene and carbon tetrachloride produces $FeCl_2$, (a) cyclopentadienyl (Cp) free radicals and (b) carbon nanoparticles (NPs) with Cl atoms at their surfaces; (c) the carbon nanoparticles can aggregate to form micrometer-sized particles with prominent tips at the surface; (d) the Cp free radicals can be immobilized at the surfaces of the carbon microparticles through a free-radical substitution reaction; (e) the immobilized Cp free radicals steadily decompose to provide carbon feed stock, which will deposit onto the prominent tips of the carbon microparticles, enwrap them with a layer of carbon, and form short carbon nanotubes; (f) with the continuous deposition of carbon feed stock, the carbon nanotubes keep growing until ferrocene are depleted.

experimental facts and depicted in Scheme 1. At elevated temperatures, ferrocene can react with carbon tetrachloride to release $FeCl_2$, cyclopentadienyl free radicals, and carbon nanoparticles with Cl atoms at their surfaces (Supporting Information Scheme S1). The tiny carbon nanoparticles (~10 nm large), having relatively high surface energies, further aggregate together through van der Waals interactions and form microsized particles with rough surfaces and irregular morphologies to decrease their total specific surface area. Meanwhile, cyclopentadienyl free radicals can be immobilized at the surfaces of the carbon microparticles through free-radical substitution reactions. The cyclopentadienyl groups become unstable under solvothermal conditions and slowly decompose to release carbon, which will preferentially deposit at the specific side of the prominent tips of the carbon microparticles with higher surface energy, scramble along the microparticle surface to the specific low-energy sides, and enwrap them with a layer of carbon. The carbon "caps" will be pushed away from the surfaces of the microparticles tips by the subsequent carbon feed stock deposition and form nanotubes with closed tips until all cyclopentadienyl groups are depleted. Moreover, some tiny carbon nanoparticles can be tightly attached to the inner surfaces of the α-CNTs through chemical bonds, break away from their loose aggregates, and get deeply into the carbon nanotubes with the deposition of carbon feed stock.

## Conclusions

In summary, formation of amorphous carbon nanotubes (α-CNTs) has been successfully demonstrated through a self-seeded surface-deposition process in the solution phase. The as-obtained α-CNTs have a high BET value of 431 $m^2\ g^{-1}$ and narrow pore-size distribution at 4.03 nm and also exhibit a steady performance with little hysteresis in lithium-ion insertion/extraction experiments as promising electrode materials at various current densities. The influence of reaction parameters on the structure and morphology of the resultant product has been investigated. The interactions among the carbon microparticles and carbon deposition play

a vital role in the whole growth process of nanotubes. A possible self-seeded surface-deposition growth mechanism of the α-CNTs is proposed. The observation is of importance to understand the nucleation process in solution and production of other tubular nanomaterials through the seeded deposition process.

**Acknowledgment.** This work was supported by the National Natural Science Foundation of China for the Key Program (20635020), the Creative Research Group (20521503), and the General Program (20773065, 20575026, and 90606016). We also are thankful for the support of the National Basic Research Program of China (2007CB936302), Modern Analysis Center of Nanjing University, and Dr. Qin Xie for EELS characterization.

**Supporting Information Available:** Figures S1−S3 and Scheme S1 (PDF). This material is available free of charge via the Internet at http://pubs.acs.org.

CM702966X